Robust strain mapping in optical coherence elastography by combining local phase-resolved measurements and cumulative displacement tracking

Vladimir Y. Zaitsev[1,2,3], Alexander L. Matveyev[1,2], Lev A. Matveev[1,2], Grigory V. Gelikonov[1,2], Ekaterina Gubarkova[2], Natalia D. Gladkova[2], and Alex Vitkin[2,4]

[1]Institute of Applied Physics Russian Academy of Sciences, Ulyanova Street 46, 603950 Nizhny Novgorod, Russia
[2]Nizhny Novgorod State Medical Academy, Minina Square 10/1, 603005 Nizhny Novgorod, Russia
[3]Nizhny Novgorod State University, Gagarina Ave. 23, 603950 Nizhny Novgorod, Russia
[4]University of Toronto and University Health Network, 610 University Ave., Toronto, Ontario, M5G 2M9, Canada

ABSTRACT

We report a novel hybrid method of robust strain mapping in compressional optical coherence elastography using combined phase measurements on sub-wavelength-scale and cumulative pixel-scale displacement tracking. This hybrid nature significantly extends the range of measurable displacements and strains in comparison with conventional direct phase-resolved measurements. As a result, the proposed strain-mapping method exhibits significantly increased robustness with respect to both additive noise and decorrelation noise produced by displacements and strains. The main advantages of the proposed approach are illustrated by numerical simulations. Experimental examples of obtained strain maps for phantoms and real biological tissues are also presented.

Keywords: optical coherence tomography, phase-resolved OCT, displacement tracking, elastography, strain mapping.

1. INTRODUCTION

Since the seminal publications of Schmidt over 15 years ago [1] the idea of utilization of optical coherence tomography (OCT) for mapping spatial distribution of the Young modulus in biological tissues (i.e., elastographic mapping by analogy with similar modality developed in medical ultrasound) has been attracted much attention. However, despite the obtained positive experience in medical ultrasound, realization of this apparently very similar idea in OCT appeared to be very challenging. In particular, under the influence of the medical ultrasound, in many works related to development of elastographic methods in OCT significant attention has been paid to the so-called compressional elastography. The main idea of this approach is to create deformation in the inspected region by the solid surface of the OCT probe itself or by an additional piston in the vicinity of which the stress field can be considered approximately uniform and uniaxial, so that the differences in the deformability of the tissue (in fact, differences in strain amplitude) in this region should characterize the differences in the stiffness of the tissue.

To characterize this difference in the tissue deformation, significant attention has been paid to utilization of correlational principles in different forms [2,3,4]. However, some features of formation of OCT images significantly complicate the application of digital image correlation to OCT scans for determining displacements of scatterers in the deformed tissue [5,6], so that some other variants of utilization of correlation principles were also discussed [7,8,9]

During the last ten years gradually the main attention in elastography-related studies in OCT turned to utilization of phase-resolved measurements for determining displacements and then extracting strains from the displacement field [10,11,12,13]. The phase variations between the reference and deformed OCT scans are intrinsically weaker distorted by

Optical Elastography and Tissue Biomechanics III, edited by Kirill V. Larin, David D. Sampson, Proc. of SPIE Vol. 9710, 97100O · © 2016 SPIE · CCC code: 1605-7422/16/$18 · doi: 10.1117/12.2211117

the deformation-induced speckle blinking and other measurement noises comparison with the distortion of the cross-correlation coefficient [5,7]. However, in the conventional measurements in inter-scan phase variations, usually one has to much stronger limit the allowable amplitude of deformations and displacements in comparison with cross-correlational methods. Indeed, conventionally, to find the phase variation between the reference and deformed OCT images, in both scans one compares pixels with the same coordinates. This is natural in the case of small, essentially sub-pixel displacements of scatterers, when both compared pixels contain the same scatterers so that the variation in the scattering-wave phases from the so-compared pixels indeed is casually related to the displacements of the scatterers. Here, for definiteness we assume that the compression of the tissue is produced by the solid output window of the common-path OCT probe, so that near the interface of the probe and the tissue the displacements of scatterers are zero and gradually increase with increasing distance from the interface. Then even for relatively small strains, say, $\leq 10^{-2}$, for which pronounced strain-induced speckle blinking yet does not occur, the displacements of scatterers in deeper regions of the deformed image can reach the pixel-scale and even supra-pixel scale as schematically illustrated in Fig. 1.

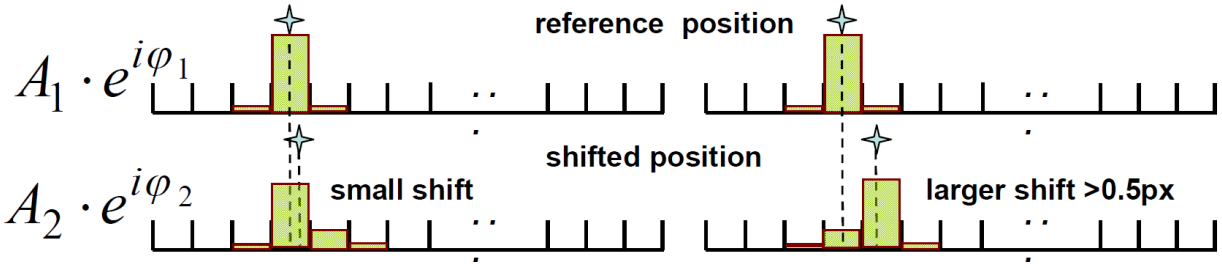

Fig. 1. Schematically shown reference (upper row) and displaced (lower row) positions of a scatter in a pixelated OCT A-scan for sub-pixel (left part of the figure) and pixel-scale (righ part of the figure) displacement of a scatterer. It is clear that for pixel-scale displacements the utilization of the same pixel coordinate strongly reduces the amplitude of the analyzed pixel in the deformed image. This makes the phase measurement prone to corruption by measurement noises. Furthermore, directly compared pixels in the case of pixel-scale displacements may even contain different scatterers with unrelated initial phases. This corresponds to appearance of strong decorrelation noise that strongly corrupts the measurement results even in the absence of any other noises.

In such a case the pixels with the same coordinates in the reference and deformed images may already contain different scatterers with unrelated phases of the scattered waves. This means that the conventionally determined phase variations based on the direct pixel-to-pixel comparison yield very noisy results even in the absence of any other noises in the measurement system. This displacement-induced decorrelation noise in conventional measurements of phase variations limits the allowable strains to fairly small values $\sim 10^{-3}$ or even smaller ones. Measurements at such small strains prevent the appearance of strong decorrelation noise, but become significantly prone to errors due to inevitable other noises in the measurement system. The usual way to reduce their masking effect is the application of period strain source and performing many-period averaging. However, for practically interesting hand-held operation by the OCT probe for *in vivo* conditions, such averaging is very problematic or completely impossible.

In what follows we demonstrate that the performed in due form tracking and compensation of pixel-scale displacements can be helpful to utilize fairly large strains (up to the onset of intense speckle blinking for strains $\sim 10^{-2}$), which can strongly enhance the quality of the determined phase-variation distribution even if the conventional pixel-to-pixel displacements yield completely noisy results. Since this method combines phase-resolved measurements and pixel-scale tracking we call this procedure Hybrid Phase-Resolved Displacement Tracking (HPRDT) method.

2. ESSENCE OF THE HRDT-APPROACH

Figure 2 illustrates the situation of gradually increasing displacement-induced decorrelation noise in the tissue compressed from the top by the surface of the OCT probe. The phase-variation is shown in the conventionally used color-encoded form and in this example is determined by conventional direct pixel-to-pixel comparison between the

reference and deformed images. In the lower part of the figure, where displacements of the scatterers are greater (and are of essentially supra-wavelength scale), the phase-variation map is pronouncedly noiser. In principle, for strong attenuation of the optical beam, the signal-to-noise ratio can noticeably diminish with increasing depth causing noiser results of phase-variation measurement. However, even for negligible decay of the optical beam, noticeable errors in pixel-to-pixel phase-variation measurement can arise due to the strain-produced translational displacements that gradually increase with increasing depth up to supra-pixel scales. Notice that the strain itself can be approximately the same over the scan, so that the noisy influence of the strain-induced speckle blinking related to the strain-produced *relative* displacements of closely located scatterers is approximately the same in the upper and lower parts of the scan (and is still weak in the discussed example). In contrast, the displacement field is inhomogeneous over the scan area and the displacement-induced decorrelation noise is negligible near the OCT-probe surface (where displacements are of essentially sub-pixel scale), but in the deeper areas the displacement is larger and the decorrelation noise becomes much stronger.

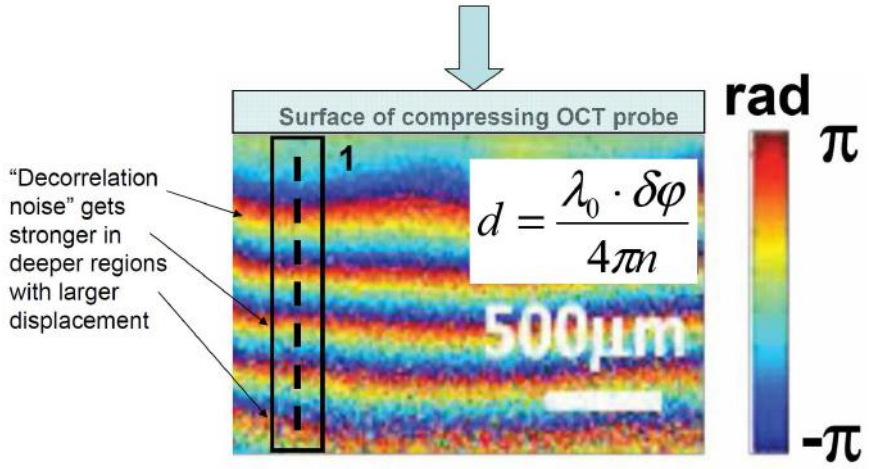

Fig. 2. Schematically shown gradual increase in the decorrelation noise with increasing depth. The decorrelation is caused by particle displacements that gradually increase with increasing depth. The tissue is compressed from the surface by the rigid surface of the OCT probe, which results in creation of strain that is approximately uniform as a function of depth in contrast to strain-produced displacement. The phase-variation is shown in the conventionally used color-encoded form. The displacement d is related to the phase variation $\delta\varphi$ as $d = \lambda_0 \delta\varphi / 4\pi n$, where λ_0 is the central wavelength of the optical source, and n is the refraction index of the tissue.

In fact if one would compare the scattered signals from the initial position of the scatterer and the pixel corresponding to its actual displaced position in the deformed image (see the right-hand part of Fig. 1), the result of such comparison can yield much more accurate result. The idea of such utilization of correcting shifts when comparing the reference and deformed images in the proposed HPRDT method is illustrated by Fig. 3.

In this approach the conventional logic of determining local strains on the basis of the initially reconstructed depth-dependence $d(z)$ of the displacements is inverted. The local strain is found by determining the local phase gradient within a chosen vertical size of the processing window. This is also advantageous for obviating the necessity of performing the error-prone procedure of phase unwrapping that is usually required for determining displacements over the entire OCT scan. Indeed, even if there occurs multiple phase-variation wrapping over the entire scan, for a much smaller processing window (say, ~10 px in the vertical direction) and typical pixel size on order of several wavelengths, the phase-variation wrapping can be unnecessary up to strains $\sim 10^{-2}$. The phase-variation gradient inside the window can be found, for example, using conventional least-square methods [11].

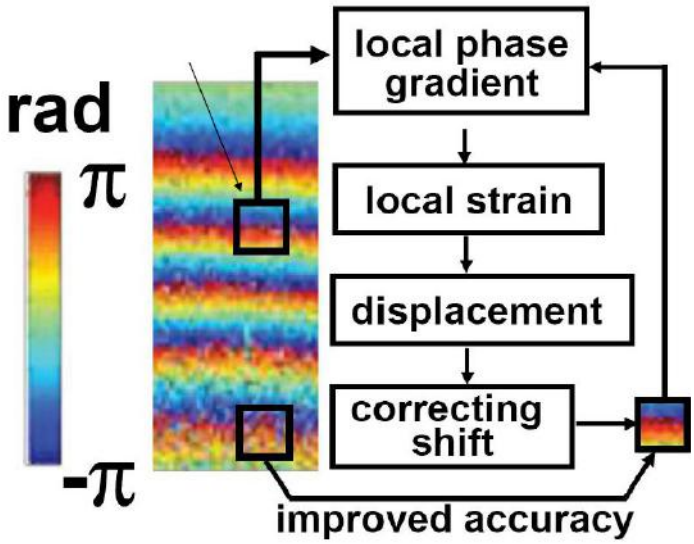

Fig. 3. Scheme of the proposed HPRDT method of the phase-variation measurement with utilization of correcting pixel-scale shifts in the regions where the displacement exceed 0.5 px, 1.5 px, etc. In the upper part of the scan conventional pixel-to-pixel comparison is made and local phase gradient with a chosen processing window are determined. For the current depth, strain-induced displacements are added to find the cumulated displacement and to verify whether the additional correcting shift should be introduced.

The values of phase gradients $\Delta\varphi_i$ rad/px determined at smaller depths can be summed to find the accumulated (unwrapped) phase variation for the qth pixel:

$$\Delta\varphi_{total}(q) = \sum_{i=1}^{q} \Delta\varphi_i \,, \tag{3}$$

This total accumulated phase variation corresponds to the accumulated displacement $d(q) = \lambda_0 \Delta\varphi_{total} / 4\pi n$. If the cumulated displacement reaches 0.5 px, 1.5 px, etc., the additional compensation one-pixel shift is introduced when comparing the phase-variation between the reference and deformed images. In what follows we demonstrate how this compensation shift can improve the accuracy of phase-variation measurement in the regions where the direct pixel-to-pixel comparison yields very noisy results.

3. DEMONSTRATION OF INCREASED ROBUSTNESS OF HPRDT METHOD WITH RESPECT TO BOTH DECORRELATION AND ADDITIVE MEASUREMENT NOISES

To demonstrate the efficiency of pixel-scale displacement tracking and its proper compensation for comparing the phase of complex-valued OCT scans even for supra-pixel displacements of scatterers, we use the model [14] to simulate the strain-induced evolution of speckle structure of OCT scans. For illustrative purposes, we do not consider depth-dependent signal decay and keep the same signal-to-noise ratio throughout the image. Also we do not consider the overlapping of A-scans in the lateral direction (which is not a principal issue for the discussed problem), so that scatterers in horizontally adjacent pixels are independent. The average density of scatterers is chosen to be 4 per pixel. As shown in [14], the shape of speckle-intensity histograms stays nearly constant for density of scatterers larger than ~2, in good agreement with properties exhibited by real OCT images. We assume that each A-scan consists of 256 pixels and the total depth of the image is 2048 μm in air. We chose that for depth $z \geq 800$ px, the material is 1.25 times softer than in the upper part, so that the strain in this deeper region is correspondingly 1.25 times greater. The central wavelength of the optical source is chosen 1300 nm and spectral width 100 nm which corresponds to the parameters of our custom-made spectral-domain OCT system and is a fairly typical value for OCT scanners.

The first example in Fig. 4 corresponds to zero additional noise and demonstrates strain reconstruction using the proposed method in the case of moderate strain (2% in the lower layer and 1.25 times smaller in the upper one). The

displacement is zero at the top of the scan increases proportionally to the depth and exceeds 4 px in the deeper part of the image, resulting in many-periods phase ambiguity over the entire depth. Panels (a-1) and (a-2) show the color-encoded phase variation between the reference and deformed scans found without and with compensating shift. It is clear that the strain-induced displacement of scatterers produces strong decorrelation between the reference and deformed images, as is shown in the correlation map Fig 4(b-1). Correspondingly, the phase-difference map Fig. 4(a-1) at larger depths demonstrates very strong displacement-induced "decorrelation noise", so that in the directly-found phase difference between the compared images [Fig. 3(a-1)] the regular phase-difference structure is completely lost. The phase-variation map in Fig. 4(a-2) shows that the compensating shift helps to significantly restore the regular phase variations, which is especially clear in the zoomed insets.

The corresponding strain maps found via fitting the phase difference between the reference and deformed-tissue images are shown in Figs.4(c-1) and (c-2) with and without compensating shift, respectively. It is clear that without the pixel-scale compensation the strain in the lower part of the image is completely corrupted by the displacement-induced decorrelation [Fig. 4(c-1)], whereas the introduced compensation makes it possible to obtain a very clear strain map [Fig. 4(c-2)]. The difference between the results obtained without and with application of the pixel-scale displacement tracking and its compensation is especially clearly seen in the callouts shown in Fig. 4.

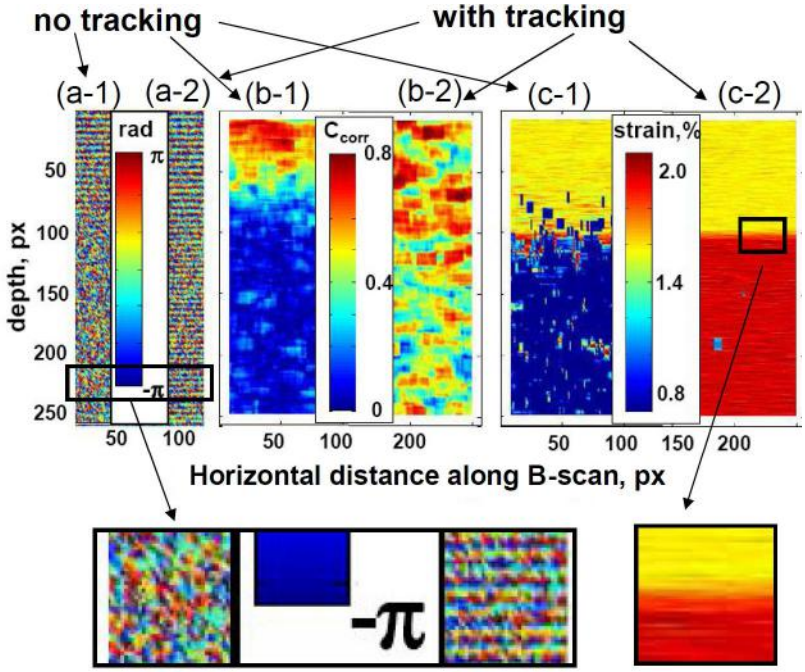

Fig. 4. Simulated example of application of the HPRDT method for mapping strain in a two-layer sample in the absence of noise. The upper layer (for z<100 px) is 1.25 times stiffer (and consequently its strain is 1.25 times smaller than the deeper layer for z>100 px). Strain in the softer deeper layer is 2%. The size of the processing window is 10 px in the vertical and 16 px in horizontal direction. whereas multiple phase-variation periods occur over the entire depth. Maximum displacement near the image bottom is over 4.5 px. Panels (a-1) and (a-2) are the phase-variation maps found without and with displacement compensation, respectively. Panels (b-1) and (b-2) are cross-correlation maps for zero-mean normalized Pearson cross-correlation coefficien C_{corr} between the compared images found without displacement compensation and with compensation, respectively. Panels (c-1) and (c-2) are strain maps found without and with interger-pixel displacement tracking, respectively.

Figure 5 shows examples of the reconstructed vertical profiles for strain and displacement found without and with pixel-scale displacement tracking and compensation. We emphasize once again that in contrast to the conventional approach, the strain distribution $s(z)$ in the upper part of the Fig. 5 is not obtained by differentiating the displacement $d(z)$, but it is the displacement which is found using summation of the strains from the upper part of the scan towards the bottom. We also note that a single profile is actually obtained for a given horizontal position of the processing window with averaging the phase difference between the reference and deformed scans over each horizontal row within the processing

window (i.e., 16 px in the discussed example). For finding the phase difference with averaging along the horizontal size of the processing window one can use, for example, the Kasai estimator [15,16] in which the contribution of noisy small-amplitude pixels to the estimated phase difference is reduced.

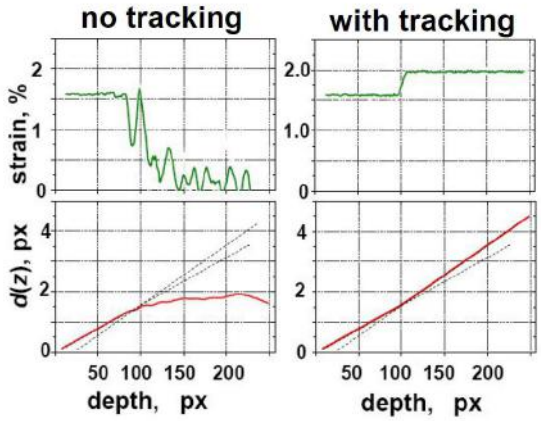

Fig. 5. Examples of single vertical profiles $s(z)$ for strain and $d(z)$ for the horizontal position $x = 100$ px found for the same simulated scans as in Fig. 4. The left part is found without displacement tracking and the right one with tracking and compensation. Dashed lines are guides for the eye showing exact slopes of $d(z)$ used in the simulation. The improvement of the reconstruction quality in the regions of supra-pixel displacement is striking.

Now we demonstrate that the displacement tracking and compensation in the HPRDT method is very useful in the presence of additional measurement noises. Figure 6 shows the plots similar to that in Figs. 4 and 5, but found with adding a rather strong random noise with average SNR=6dB over the simulated reference and deformed scans.

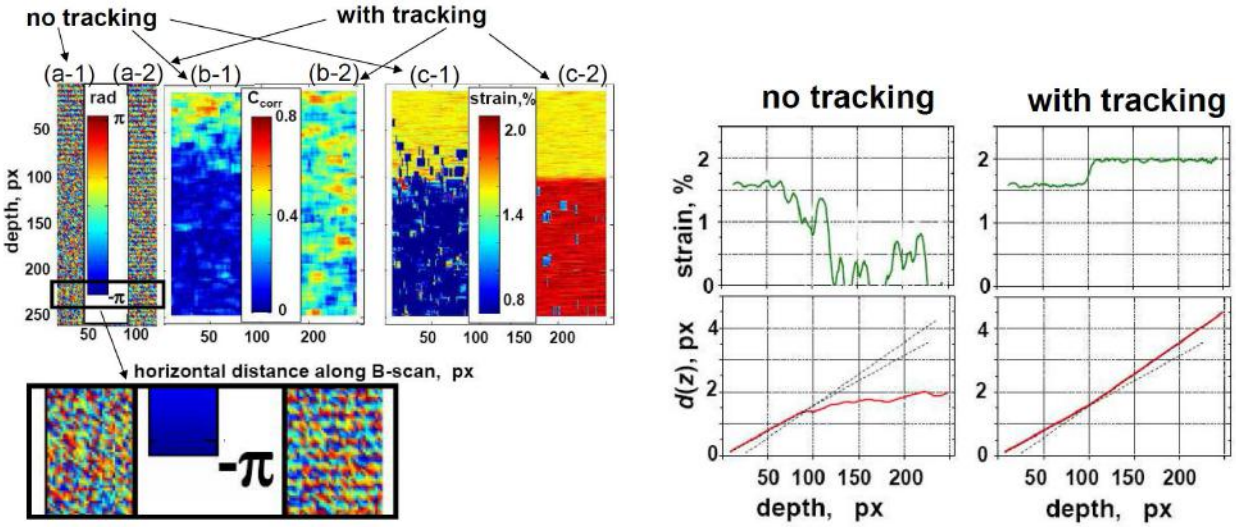

Fig. 6. Simulated example of application of the HPRDT method for mapping strain in a two-layer sample in the presence of rather strong noise with SNR=6 dB and the same other parameters as for Figs. 4 and 5. Panels (a-1) and (a-2) are the phase-variation maps found without and with displacement compensation by integer number of pixels, respectively. Panels (b-1) and (b-2) are cross-correlation maps for zero-mean normalized Pearson cross-correlation coefficient C_{corr} between the compared images found without displacement compensation and with compensation, respectively. Panels (c-1) and (c-2) are strain maps found without and with integer-pixel displacement tracking, respectively.

The callout in Fig. 6 clearly shows that despite the presence of rather strong noise, the apparently absent regular structure of phase variations in the lower part of the scan corresponding to supra-pixel displacements can be efficiently recovered

by applying the pixels-scale displacement tracking and compensation. Then the quality of the reconstructed depth dependences $s(z)$ and $d(z)$ becomes comparable with the results shown in Figs. 4 and 5 that are obtained for zero noise.

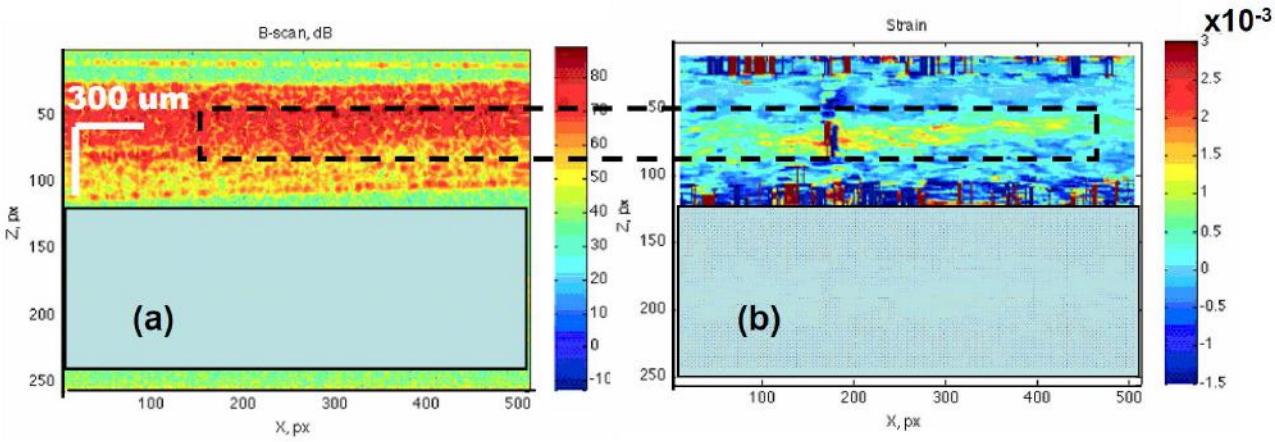

Fig. 7. A real example demonstrating that the strain map obtained by the developed method based on fitting local strain gradients is able to reveal structural features of the sample that are not distinguishable in the conventional morphological image. Panel (a) is such a conventional structural image of a hamster's cheek-pouch tissue representing two layers of the pouch wall one above another. The interface between the two layers indistinguishable in the structural scan is clearly visualized as an inter-layer with increased strain in the strain map shown in panel (b) (see the region labelled by the dashed-line rectangle). The lower parts of both plots are intentionally masked since the signal in these region is exclusively due to system noises. The processing-window size is 10 px in the vertical and 16px in the horizontal direction.

Next we demonstrate some examples of obtaining real elastographic maps using the OCT scanner with parameters close to those used in the simulations. Figure 7 shows a structural B-scan for a humster's cheek pouch in the normal state places onto a rubber opaque substrate. The lower parts of both panels in Fig. 7 is masked, because the signal in this region is completely due to system noises. The structural scan clearly shows the region of the tissue that actually represents the two layers of the cheek-pouch, one above another. The tissue of the pouch is strongly scattering so that the gradual signal attenuation is clearly seen in the structural image Fig. 7a, but the boundary between the two layers is not distinguishable at the structural image. However, in the strain map shown in Fig. 7b, there is a clearly seen zone of increased strain in the middle height of the tissue image (indicated by the dashed-line rectangle), where the two cheek-pouch layers touch each other and this contact region is stronger deformable. The two compared B-scans used for obtaining the strain map in Fig. 7b were obtained by pressing the OCT probe onto the tissue in the hand-controlled regime. This example is chosen to demonstrate that the strain map obtained by the proposed method is helpful for revealing such features of the tissue that are not visible in the structural scan (the presence of an interface between to layers). Due to the type of the chosen sample with *a priori* known two-layer structure one can be sure that the interface region revealed in the strain map is real (not an artifact due to the processing produces).

4. CONCLUSIONS

The proposed hybrid method of strain mapping in OCT combines advantages of conventionally used phase-resolved measurements of displacements at a sub-wavelength scale and displacement tracking at a greater the pixel-size scale. The latter scale is more typical of correlational speckle tracking.

The displacement range measured in conventional phase-resolved methods is significantly restricted by the problem of phase-variation wrapping (that occurs in OCT for displacements > $\lambda_0 / 2$), as well as by significant corruption of the phase-measurement accuracy induced by pixel-scale and greater displacements. Although in comparison with phase methods, correlational displacement tracking potentially allows for measuring larger displacements, the accuracy of correlational tracking is significantly stronger degraded by both additive noises in the OCT system and decorrelation noises cause by strain-induced speckle blinking. The proposed way of cumulatively determining supra-wavelength

displacements is much more tolerant to both decorrelation and additive noises as illustrated in Fig. 6. The corresponding comparative examples and other details will be published elsewhere.

The proposed way of compensating the displacement-induced decorrelation noises in the proposed HPRDT method makes it operable up to significantly greater strains than conventional phase-resolved methods based on the direct pixel-pixel comparison. Since in elastograpy the interest represents strain directly related to phase gradient rather than cumulative displacements, the possibility of utilization greater strains ensures greater strain gradients and, therefore (for a given measurement-noise level) enhances the effective signal-to-noise ratio in the problem of strain mapping. This makes the strain-mapping procedure in the HPRDT method exceptionally tolerant to noises.

The latter property opens the possibility to obtain fairly clear strain maps by utilizing a single pair of compared OCT scans without the necessity of the strain-map quality enhancement by application of stable periodic sources of straining and many-period averaging. This feature of the method is especially interesting for potential clinical applications for which the tissue straining can be produced by the OCT probe in the hand-held regime.

5. ACKNOWLEDGEMENTS

The study was supported by the Russian Science Foundation grant No 14-15-00538. Fabrication of the custom-made OCT equipment used in the experiments was funded by the Russian Federation Government contract No 14.B25.31.0015 for Leading Scientists to Russian Educational Institutions. L.A.M acknowledges the support of the Russian President grant for young scientists No MK-6504.2016.2 and RFBR grant No 16-02-00642.

REFERENCES

[1] Schmitt, J. M., "OCT elastography: imaging microscopic deformation and strain of tissue," *Optics express*, **3**(6), 199-211 (1998).
[2] Rogowska, J., Patel, N., Fujimoto, J. G., & Brezinski, M. E., "OCT elastography of the vascular tissue-importance of cross-correlation kernel size". In *Biomedical Topical Meeting* (p. PD20). Optical Society of America (2002).
[3] Rogowska, J., Patel, N. A., Fujimoto, J. G., & Brezinski, M. E., "Optical coherence tomographic elastography technique for measuring deformation and strain of atherosclerotic tissues". *Heart*, *90*(5), 556-562 (2004).
[4] Sun, C., Standish, B., & Yang, V. X., "Optical coherence elastography: current status and future applications," *Journal of biomedical optics*, **16**(4), 043001-043001 (2011).
[5] Zaitsev, V. Y., Gelikonov, V. M., Matveev, L. A., Gelikonov, G. V., Matveyev, A. L., Shilyagin, P. A., & Vitkin, I. A., "Recent trends in multimodal optical coherence tomography. I. Polarization-sensitive OCT and conventional approaches to OCT elastography," *Radiophysics and Quantum Electronics*, **57**(1), 52-66 (2014).
[6] Zaitsev, V. Y., Matveyev, A. L., Matveev, L. A., Gelikonov, G. V, Gelikonov, V. M., & Vitkin, A., "Deformation-induced speckle-pattern evolution and feasibility of correlational speckle tracking in optical coherence elastography," *J. Biomed. Opt.*, **20**(7), 075006(1–12), http://doi.org/10.1117/1.JBO.20.7.075006 (2015).
[7] Zaitsev, V. Y., Vitkin, I. A., Matveev, L. A., Gelikonov, V. M., Matveyev, A. L., & Gelikonov, G. V., "Recent Trends in Multimodal Optical Coherence Tomography. II. The correlation-stability approach in OCT elastography and methods for visualization of microcirculation," *Radiophysics and Quantum Electronics*, **57**(3), 210–225 (2014).
[8] Zaitsev, V. Y., Matveev, L. A., Gelikonov, G. V., Matveyev, A. L., & Gelikonov, V. M., "A correlation-stability approach to elasticity mapping in optical coherence tomography," *Laser Physics Letters*, **10**(6), 065601 (2013).
[9] Zaitsev, V. Y., Matveev, L. A., Matveyev, A. L., Gelikonov, G. V., & Gelikonov, V. M., "Elastographic mapping in optical coherence tomography using an unconventional approach based on correlation stability," *Journal of biomedical optics*, **19**(2), 021107 (2014).
[10] Wang, R. K., Kirkpatrick, S., & Hinds, M., "Phase-sensitive optical coherence elastography for mapping tissue microstrains in real time," *Applied Physics Letters*, **90**(16), 164105 (2007).
[11] Kennedy, B. F., Koh, S. H., McLaughlin, R. A., Kennedy, K. M., Munro, P. R., & Sampson, D. D. "Strain estimation in phase-sensitive optical coherence elastography," *Biomedical optics express*, **3**(8), 1865-1879(2012).
[12] Kennedy, B. F., Kennedy, K. M., & Sampson, D. D., "A review of optical coherence elastography: fundamentals, techniques and prospects," *IEEE Journal of Selected Topics in Quantum Electronics*, **20**(2), 272-288 (2014).

[13] Chin, L., Curatolo, A., Kennedy, B. F., Doyle, B. J., Munro, P. R., McLaughlin, R. A., & Sampson, D. D., "Analysis of image formation in optical coherence elastography using a multiphysics approach," *Biomedical optics express*, **5**(9), 2913-2930 (2014).
[14] Zaitsev, V. Y., Matveev, L. A., Matveyev A. L., Gelikonov, G. V, and Gelikonov, V. M., "A model for simulating speckle-pattern evolution based on close to reality procedures used in spectral-domain OCT," Laser Phys. Lett. **11**, 105601 (2014).
[15] Kasai, C., Namekawa, K., Koyano, A., and Omoto, R., "Real-time two-dimensional blood flow imaging using an autocorrelation technique," IEEE Trans. Son. Ultrason., **32**, 458 (1985).
[16] Matveev, L. A., Zaitsev, V. Y., Gelikonov, G. V, Matveyev, A. L., Moiseev, A. A., Ksenofontov, S. Y., V. M. Gelikonov, M. A. Sirotkina, N. D. Gladkova, V. Demidov, A. Vitkin, A., "Hybrid M-mode-like OCT imaging of three-dimensional microvasculature in vivo using reference-free processing of complex valued B-scans," *Optics Letters*, **40**(7), 1472–1475. http://doi.org/http://dx.doi.org/10.1364/OL.40.001472 (2015).